



#### RESEARCH ARTICLE

# Robust fractional-order adaptive gain-scheduled control strategy for civil unmanned aerial vehicle with LPV models

S. Kissoum<sup>1</sup> and S. Ladaci<sup>2</sup>

Corresponding author: Samir Ladaci; Email: samir.ladaci@g.enp.edu.dz

Received: 2 January 2025; Revised: 21 September 2025; Accepted: 23 September 2025

Keywords: altitude; FOPID controller; gain-scheduling; LQR controller; LPV system; robust control; UAV; velocity

#### Abstract

Recently, autonomous aerial systems have received unparalleled popularity and applications as varied as they are innovative in the civil domain. The unmanned aerial vehicle (UAV) is now the subject of intensive research in both aeronautical and automotive engineering.

This paper presents a new, robust gain-scheduled adaptive control strategy for a class of UAV with linear parameter varying (LPV) models. The proposed controller synthesis involves a set of pre-tuned linear quadratic regulator (LQR) combined with fractional-order PID controllers supervised with an adaptive switching law. The main innovation in this work is the enhancement of the classical gain-scheduling adaptive control robustness for systems with LPV models by combining a set of robust LQR + fractional-order PID compensators. The stability of the resulting controller is demonstrated and its efficiency is validated using a numerical simulation example on a civilian UAV system airspeed and altitude control to illustrate its practical efficiency and achieved robustness.

#### Nomenclature

AFCS autonomous flight control system  $C_{\scriptscriptstyle M}$ pitching moment coefficient  $C_{r}$ axial force-body axis  $C_z$ normal force-body axis **FOPID** fractional-order PID controller GSgain-scheduling

h altitude

 $J_{i}(t)$ cost function for the switching law  $J_{\scriptscriptstyle LOR}$ performance index for LQR control

LPVlinear parameter varying linear quadratic regulator LOR Μ moment along aircraft Y-axis

m UAV mass

PID proportional-integral-derivative controller p angular velocity along aircraft X-axis angular velocity along aircraft Y-axis

S UAV mass

UAV unmanned aerial vehicle

angular velocity along aircraft Z-axis

S wing area

area swept by the propeller

<sup>&</sup>lt;sup>1</sup>Department of E.E.A. GEPC Laboratory, National Polytechnic School of Constantine, Constantine, Algeria

<sup>&</sup>lt;sup>2</sup>Department of Automatic Control Engineering, Ecole Nationale Polytechnique, Algiers, Algeria

<sup>©</sup> The Author(s), 2025. Published by Cambridge University Press on behalf of Royal Aeronautical Society. This is an Open Access article, distributed under the terms of the Creative Commons Attribution licence (https://creativecommons.org/licenses/by/4.0/), which permits unrestricted re-use, distribution and reproduction, provided the original article is properly cited.

#### 2 Kissoum and Ladaci

SPSA simultaneous perturbation stochastic approximation u a scalar and represents linear velocity along  $X_b$   $u_c$  vector of control signal  $V_{air}$  airspeed

## Greek Symbol

α angle-of-attack δ. elevator deflection angle throttle opening  $\delta_T$  $\Gamma$  (.) Gamma function roll angle φ yaw angle ψ linear velocity along aircraft Z-axis (ı) ρ air density θ pitch angle

#### 1.0 Introduction

Gain-scheduling (GS) technique is one standard option to resolve the control problem of nonlinear and time-varying systems. This technique has been omnipresent in the literature of automatic theory since the 1960s. Indeed, for many dynamic systems, the model varies over time, which prohibits the use of classic control techniques [1–3]. Early attempts at control used adaptive control, which was popular at the time [4]. However, the major drawback of this control technique is that it only ensures stability for systems whose parameters vary relatively slowly. To overcome this defect, other researchers have turned to robust control [5]; but many others preferred the LPV gain-scheduling (GS) command, which makes it possible to process continuous or discontinuous variations in the parameters of the controlled process model. Many applications are available in specialised literature [6, 7].

Besides, robust control is the control method that is able to counteract uncertainties in a process. It can be used as an attempt to maintain a certain level of performance for the closed-loop LPV system despite uncertainties and disturbances. One of the most popular robust control techniques is LQR control [8, 9]. This robust control solution has been intensively applied to UAV systems [10, 11].

Moreover, applications of fractional calculus in various engineering fields have attracted a huge research effort over the last years [12, 13]. Several recent works and results have shown the ability of fractional order operators to better represent and simulate certain physical phenomena and to increase the precision and speed in addition to the robustness of control systems [14, 15].

This is why many researchers have proposed their use in the supervision of industrial processes [16, 17]. They take advantage of this advantageous property of fractional order systems, which is long memory in addition to incomparable dynamic properties [18, 19]. This is how fractional control makes it possible to obtain superior results in terms of temporal responses and robustness against measurement noise and parametric disturbances [20, 21].

At the same time, many researchers are currently interested in UAVs regarding their control as well as their configuration and aerodynamics. A particular type of UAV is flying wings, which have a better aerodynamic coefficient. But this comes at the cost of making robust control design more difficult because it is very sensitive to variations in control signals.

New methods [22–24] based on artificial intelligence were proposed to redesign of morphing (i.e. varying arm length) UAV for improvement of the index consisting of directional stability and maximum lift/drag (L/D) ratio. Whereas in Ref. (25) they used simultaneous perturbation stochastic approximation (i.e. SPSA), deep neural network and PID controller according to morphing.

More recently some authors [26, 27] proposed to improve the UAV flight performance by simultaneously and stochastically redesigning its vertical tail and autonomous flight control system (AFCS). Many other works focused on new control strategies for UAV manoeuvering and landing [28, 29].

In this study, an application of a robust gain scheduled LPV LQR + fractional-order PID controller (FOPID) control structure is proposed for a class of UAV with LPV models.

The structure of this paper is as follows. In Section 2, the UAV model is presented. In Section 3, some fundamental definitions of fractional-order systems and FOPID control are introduced. Section 4 presents the LQR control configuration. In Section 5, the robust gain-scheduled control with the switching law based on a moving performance index is introduced. In Section 6, numerical simulations of the application of the proposed solution for UAV system control is provided to demonstrate its effectiveness, even in presence of additive random noises. At the end, some concluding comments are given in Section 7.

#### 2.0 Uav modelisation

UAVs are attracting great interest for their guidance and control, particularly in view of the control techniques [7]. So their configuration and modeling is important for a more efficient design. In this work we consider flying wings, which are more profitable in terms of aerodynamic coefficient.

A linearised equation of motion can be obtained based on the small-disturbance theory [30, 31].

The main idea is to linearise the model around a steady-state condition (trimmed flight). Assuming that deviations from this equilibrium state are small, a linearised model is expected to provide useful and fairly accurate representation of the nonlinear system.

In this theory, each variable in the model is assumed to have a nominal value (at trimmed flight, indexed 0), plus a disturbance value; for instance,  $u_0$  is the nominal value for linear velocity along body  $X_b$  axis, and  $\Delta u$  is the small perturbation.

The equation of motion of the plane is derived from the Newton's Second Law of motion. The relationships between forces in the body frame  $(F_X, F_Y, F_Z)$ , moments (L, M, N) and aircraft linear (u, v, w) and angular (p; q; r) velocities.

$$F_X = m \left( \dot{u} + qw - rv \right)$$

$$F_Y = m \left( \dot{v} + ru - pw \right)$$

$$F_Z = m \left( \dot{w} + pv - qw \right)$$
(1)

$$L = I_{x}\dot{p} - I_{xz}\dot{r} + qr(I_{z} - I_{y}) - I_{xz}pq$$

$$M = I_{y}\dot{q} + rp(I_{x} - I_{z}) + I_{xz}(p^{2} - r^{2})$$

$$N = -I_{xz}\dot{p} + I_{z}\dot{r} + pq(I_{y} - I_{x}) + I_{xz}qr$$
(2)

where m is the UAV mass, g is the gravitational acceleration and is  $\approx 9.8/s^2$ .

Force and moment components can be decomposed in three sub-components of thrust (created by aircraft engine), gravitational (due to the earth gravity) and aerodynamic (produced due to the governing rules of aerodynamics) [34].

When expressed in the body frame, the gravitational force is a function of aircraft orientation in space and depends on pitch  $(\theta)$  and roll  $(\phi)$  angles. The gravity creates no moment since it acts through the UAV center of gravity. Force components due to gravity expressed in body frame, can be computed as:

$$(F_X)_{gravity} = -mg \sin(\theta)$$

$$(F_Y)_{gravity} = mg \cos(\theta) \sin(\phi)$$

$$(F_Z)_{gravity} = mg \cos(\theta) \cos(\phi)$$
(3)

where  $\theta$  and  $\phi$  are aircraft pitch and roll angles, respectively. Assume that the sum of aerodynamic and thrust forces are X, Y and Z. Force components due to gravity expressed in body frame, can be computed as:

4

$$X - mgsin(\theta) = m(\dot{u} + qw - rv)$$

$$Y + mgcos(\theta)sin(\phi) = m(\dot{v} + ru - pw)$$

$$Z + mgcos(\theta)cos(\phi) = m(\dot{w} + pv - qw)$$
(4)

Equation (4) represent the dynamics and kinematics of the UAV.

If we consider X (the force along the body  $X_b$  axis) as described in Equation (4). By introducing the small-disturbance notation into this equation and simplifying the result, following equation will be obtained as,

$$\Delta X - mg \,\Delta\theta \,\cos\theta_0 = m \,\Delta\dot{u} + m \,w_0 \,\,\Delta q \tag{5}$$

Where  $\Delta X$  is the change in the force along the  $X_b$  direction (contribution of aerodynamic force and thrust). It is possible to express  $\Delta X$  in terms of perturbation variables using Taylor series [32].

Considering the longitudinal axis, the X force equation can be rewritten as

$$\dot{u} = rv - qw - g\sin\theta + \frac{X}{m} \tag{6}$$

where X represents the combination of aerodynamic and propulsive forces (i.e.  $X = F_{X_{aero}} + F_{X_{prop}}$ ). Assuming that Ref. (33)  $\phi = p = r = \beta = v = 0$ ,  $F_{X_{aero}}$  and  $F_{X_{prop}}$  can be computed as:

$$F_{X_{aero}} = \frac{\rho (u^2 + w^2) S}{m} \left[ C_{x_0} + C_{x_\alpha} \alpha + C_{x_{\delta_e}} \delta_e \right] + \frac{\rho \sqrt{u^2 + w^2} S}{m} C_{X_q} \hat{c} q$$

$$F_{X_{prop}} = \frac{1}{2} \rho S_{prop} ((K_{motor} \delta_T)^2 - V_{air}^2)$$
(7)

where  $\rho$  is the air density, u and w are velocities along body x-axis and z-axis, respectively,  $C_{X_0}$  is the axial force coefficient,  $C_{X_{\alpha}}$  is the derivative of the axial force with respect to  $\alpha$ ,  $C_{x_{\delta_e}}$  is the derivative of the axial force with respect to  $\delta_e$  and  $\hat{c}$  is the wing chord.

Substituting back Equation (7) into (6) with the assumption that  $\phi = p = r = \beta = v = 0$ , we will get:

$$\dot{u} = -qw - gsin\theta + \frac{\rho (u^2 + w^2) S}{m} \left[ C_{x_0} + C_{x_\alpha} \alpha + C_{x_{\delta_e}} \delta_e \right] + \frac{\rho \sqrt{u^2 + w^2} S}{m} C_{X_q} \hat{c} q + \frac{1}{2} \rho S_{prop} ((K_{motor} \delta_T)^2 - V_{air}^2)$$
(8)

This procedure should be repeated for all non-linear forces and moments. The results (longitudinal terms) would be as follows (see Fig. 1) [34]:

$$\begin{cases}
\dot{u} = -qw - g\sin\theta + \frac{\rho(u^2 + w^2)s}{2m} \left[ C_{x_0} + C_{x_\alpha}\alpha + C_{x_{\delta_e}}\delta_e \right] + \frac{\rho\sqrt{u^2 + w^2s}}{2m} C_{x_q}\hat{c}q \\
+ \frac{1}{2m}\rho s_{prop}((k_{motor}\delta_T)^2) - V_\alpha^2 \right) \\
\dot{w} = -qu - g\cos\theta\cos\phi + \frac{\rho(u^2 + w^2)s}{2m} \left[ C_{z_0} + C_{z_\alpha}\alpha + C_{z_{\delta_e}}\delta_e \right] + \frac{\rho\sqrt{u^2 + w^2s}}{2m} C_{z_q}\bar{c}q \\
\dot{q} = \frac{1}{2I_y}\rho(u^2 + w^2)\bar{c}s \left[ C_{m_0} + C_{m_\alpha}\alpha + C_{m_{\delta_e}}\delta_e \right] + \frac{1}{2I_y}\rho\sqrt{u^2 + w^2}\bar{c}s C_{m_q}\bar{c}q \\
\dot{\theta} = q\cos\phi - r\sin\phi = q
\end{cases} \tag{9}$$

In order to obtain an operational model, we will use the so-called small-disturbance method. It means that the variables are replaced by their nominal values plus a small disturbance value, then by taking a

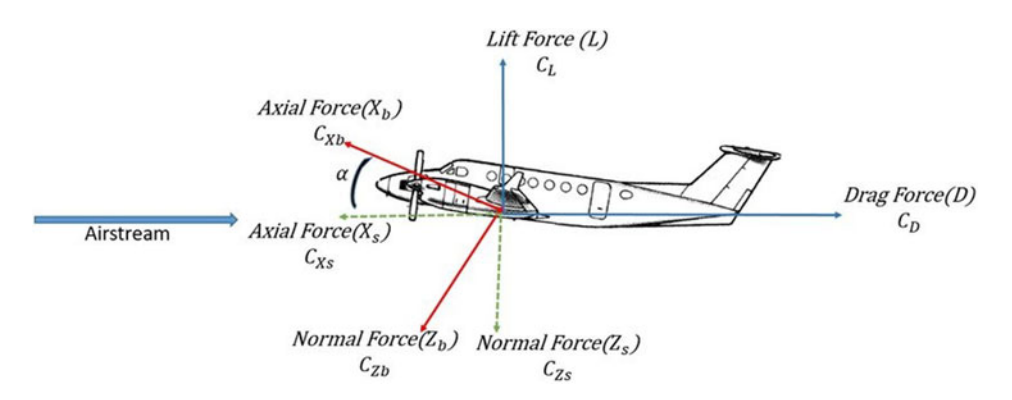


Figure 1. UAV forces in stability and body axes.

linear approximation we obtain the following equations using the Jacobians:

$$\frac{df}{dx} = \begin{bmatrix}
\frac{\partial \dot{u}}{\partial u} & \frac{\partial \dot{u}}{\partial w} & \frac{\partial \dot{u}}{\partial q} & \frac{\partial \dot{u}}{\partial \theta} \\
\frac{\partial \dot{w}}{\partial u} & \frac{\partial \dot{w}}{\partial w} & \frac{\partial \dot{w}}{\partial q} & \frac{\partial \dot{w}}{\partial \theta} \\
\frac{\partial \dot{q}}{\partial u} & \frac{\partial \dot{q}}{\partial w} & \frac{\partial \dot{q}}{\partial q} & \frac{\partial \dot{q}}{\partial \theta} \\
\frac{\partial \dot{\theta}}{\partial u} & \frac{\partial \dot{\theta}}{\partial w} & \frac{\partial \dot{\theta}}{\partial q} & \frac{\partial \dot{\theta}}{\partial \theta}
\end{bmatrix}$$
(10)

$$\frac{df}{du_c} = \begin{bmatrix}
\frac{\partial \dot{u}}{\partial \delta_e} & \frac{\partial \dot{u}}{\partial \delta_T} \\
\frac{\partial \dot{w}}{\partial \delta_e} & \frac{\partial \dot{w}}{\partial \delta_T} \\
\frac{\partial \dot{q}}{\partial \delta_e} & \frac{\partial \dot{q}}{\partial \delta_T} \\
\frac{\partial \dot{\theta}}{\partial \delta_e} & \frac{\partial \dot{\theta}}{\partial \delta_T}
\end{bmatrix} \tag{11}$$

Note that  $u_c$  is a vector of control signal  $u_c = [\delta_e \ \delta_T]^T$ , where  $\delta_e$  is the elevator deflection angle and  $\delta_T$  is the throttle opening, such that u is a scalar and represents linear velocity along  $X_b$ , w is the linear velocity along aircraft Z-axis,  $\theta$  is the pitch angle and q is the angular velocity along aircraft Y-axis.

The UAV system outputs are the airspeed  $V_{air}$  and the altitude h.

However, controlled outputs are airspeed  $\Delta V_{air}$  and aircraft's height  $\Delta h$ .

Finally, longitudinal linearised model will be given by:

$$\Delta \dot{u} = X_u \Delta u + X_w \Delta w + X_q \Delta q - g \cos \theta \Delta \theta + X_{\delta_e} \Delta \delta_e + X_{\delta_T} \Delta \delta + w_0 \Delta q$$

$$\Delta \dot{w} = Z_u \Delta u + Z_w \Delta w + Z_q \Delta q - g \sin \theta \Delta \theta + Z_{\delta_e} \Delta \delta_e + w_0 \Delta q$$

$$\Delta \dot{q} = M_u \Delta u + M_w \Delta w + X_q \Delta q + M_{\delta_e} \Delta \delta_e$$

$$\Delta \dot{\theta} = \Delta q$$
(12)

Formula  $\frac{\frac{\rho s}{m} \left[ C_{x_0} + C_{x_{\alpha}} \alpha + C_{x_{\delta,e}} \delta_e \right] - \frac{\rho s_{wc_{x_{\alpha}}}}{2m} - \frac{\rho S_{prop} C_{prop} u}{m}}{m}$ Longitudinal Derivatives  $X_u$  $\frac{u\rho s}{m}\left[C_{x_0}+C_{x_{\alpha}}\alpha+C_{x_{\delta_e}}\delta_e\right]-\frac{\rho swc_{x_{\alpha}}}{2m}-\frac{\rho Sp_oC_{prop}u}{m}$  $X_{w}$  $-w+\frac{\rho V_{\alpha}SC_{X_q}c}{2m}$  $X_q$  $\frac{\rho \ V^2 S C_{X_{\delta_e}} \, c}{2m}$  $X_{\delta_a}$  $X_{\delta \tau}$  $\frac{u\rho s}{m} \left[ C_{Z_0} + C_{Z_{\alpha}} \alpha + C_{Z_{\delta_a}} \delta_e \right] - \frac{\rho s w c_{Z_{\alpha}}}{2}$  $Z_u$  $\frac{u\rho s}{m} \left[ C_{Z_0} + C_{Z_{\alpha}} \alpha + C_{Z_{\delta}} \delta_e \right] - \frac{\rho s w c_{Z_{\alpha}}}{2m}$  $Z_{w}$  $u + \frac{\rho V_{\alpha} S C_{Z_q} c}{2 \cdots}$  $Z_a$  $Z_{\delta_e}$  $\frac{u\rho\left[{}_{M_0}+C_{M_\alpha}\alpha+C_{M_{\delta_e}}\delta_e\right]}{J_{\scriptscriptstyle V}}\;-\;\frac{\rho S_c C_{M_\alpha}w}{2J_{\scriptscriptstyle V}}$  $M_{ii}$  $\frac{u\rho s \left[ C_{M_0} + C_{M_\alpha} \alpha + C_{M_{\delta_e}} \delta_e \right]}{J_y} - \frac{\rho S_c C_{M_\alpha} u}{2J_y} \frac{\rho V S C^2 C_{M_q}}{2J_y}$  $M_w$  $M_a$  $\frac{\rho V^2 ScC_{M_{\delta_e}}}{2J_v}$  $Z_{\delta_e}$ 

**Table 1.** Longitudinal stability derivatives

**Remark:** The procedure for obtaining this linearised model and its validation for the different output variables as a function of the approximation error is detailed in the reference book [32].

## 2.1 State-space representation of the linearised model

Linearised equations are based on simple linear ordinary differential equations. The parameters are given in Table 1, and the numerical values for longitudinal stability derivatives are presented in Table 2 [35].

With  $\rho$ ,  $C_M$ ,  $C_x$ ,  $C_z$ , M, m, p, S+ and  $S_{prop}$  are air density, pitching moment coefficient, axial forcebody axis, normal force-body axis, moment along aircraft Y-axis, UAV mass, angular velocity along aircraft X-axis, wing area and area swept by the propeller, respectively. We are now able to transform them into a state space model with a number of ordinary first-order differential equations [9].

The description of the UAV longitudinal movement is described by a set of three equations:

$$\begin{bmatrix} \Delta \dot{u} \\ \Delta \\ \Delta \dot{q} \\ \Delta \dot{\theta} \end{bmatrix} = \begin{bmatrix} X_u & X_w & X_q + w_0 & -g\cos\theta_0 \\ Z_u & Z_w & Z_q - w_0 & -g\sin\theta_0 \\ M_u & M_w & M_q - w_0 & 0 \\ 0 & 0 & 1 & 0 \end{bmatrix} \begin{bmatrix} \Delta u \\ \Delta w \\ \Delta q \\ \Delta \theta \end{bmatrix} + \begin{bmatrix} X_\delta & X_{\delta_e} \\ Z_{\delta_e} & 0 \\ M_{\delta_e} & 0 \\ 0 & 0 \end{bmatrix} \begin{bmatrix} \Delta_{\delta_e} \\ \Delta_{\delta_T} \end{bmatrix}$$
(13)

Variable	<i>X</i> -Force	Z-Force	<i>M</i> -Moment
	Derivative	Derivative	Derivative
u	$X_u = -0.0543$	$Z_u = -2.7791$	$M_u = -0.3403$
w	$X_w = -0.5332$	$Z_w = -10.3435$	$M_w = -2.0302$
$\delta_e$	$X_{\delta_e} = 2.4224$	$Z_{\delta_e} = -20.2054$	$M_{\delta_e} = -18.4384$
$\delta_T$	$X_{\delta_T} = 0.0224$	$Z_{\delta_T} = -0.0020$	$M_{\delta_T}=0$

**Table 2.** Numerical values for longitudinal stability derivatives

**Table 3.** Trim condition values

Variable	Value	
0	9,7 m/s	
$v_0$	0 m/s	
$w_0$	1, 2 m/s	
$lpha_0$	$6,9^{\circ}$	
$V_0$	$10 \ m/s$	
$H_0$	150 m	
$\theta_0$	$6,9^{\circ}$	

Table 3 tabulates trim condition values. It is possible to compute small variations in each force and moment element  $(\Delta X, \Delta Y, \Delta Z, \Delta L, \Delta M, \Delta N)$  as an effect of variation in a particular variable  $(u, w, \delta, ...)$  [36]:

In this equation, the zero index denotes the trimmed light condition ( $\theta_0$  is the pitch angle for trim condition,  $u_0$  is the linear velocity along body  $X_b$  axis etc.).

## 2.2 LPV model based on the angle-of-attack α

In order to obtain the LPV model set, we consider the scheduling variable here as the angle-of-attack  $\alpha$  as mentioned in Table 1. By taking five different values of the parameter  $\alpha$  (which can be considered as the centres of five intervals of variation for the angle-of-attack), we obtain five state-space models reported in Table 4.

#### 3.0 Fractional-order pid controller

Since the early days of fractional calculus theory, many have seen the value of this new tool in improving and positively affecting all aspects of modern engineering. The mathematical definitions of fractional order differentiation are numerous and diverse, the best known and used of which are those of Grünwald-Letnikov, Riemann-Liouville and Caputo [37].

# 3.1 Definition of fractional integration

Riemann-Liouville definition for non-integer integral is the following:

$$D_a^{-\nu} f(t) = \frac{1}{\Gamma(\nu)} \int_a^t (t - \zeta)^{\nu - 1} f(\zeta) d(\zeta)$$
 (14)

with the Gamma function presented as

$$\Gamma(x) = \int_0^\infty y^{x-1} e^{-y} dy,$$
 (15)

such that  $(a, t) \in \Re^2$  with a < t and  $(0 < v < 1, v \in \Re)$ .

Parameter  $\alpha$ State-space model  $\alpha = 6.9^{\circ} \qquad A_0 = \begin{bmatrix} 59.0304 & 11.6281 & 0 & -7.9941 \\ -123.7992 & -24.4026 & 8.5 & -5.6687 \\ -27.0104 & -5.3389 & 0 & 0 \\ 0 & 0 & 1 & 0 \end{bmatrix}, B_0 = \begin{bmatrix} 11.8420 & 0.0224 \\ -16.7239 & 0 \\ -18.5670 & 0 \\ 0 & 0 \end{bmatrix}$  $\alpha = 7.5^{\circ} \qquad A_{1} = \begin{bmatrix} 128.9026 & 24.6476 & 0 & -7.9941 \\ -74.8118 & -14.3128 & 8.5 & -5.6687 \\ -29.3712 & -5.3389 & 0 & 0 \\ 0 & 0 & 1 & 0 \end{bmatrix}, B_{1} = \begin{bmatrix} 19.2166 & 0.0224 \\ -7.1163 & 0 \\ -18.5670 & 0 \\ 0 & 0 & 0 \end{bmatrix}$  $\alpha = 7.9^{\circ} \qquad A_2 = \begin{bmatrix} 155.7253 & 29.2486 & 0 & -7.9941 \\ -19.7026 & -3.7076 & 8.5 & -5.6687 \\ -30.9450 & -5.8256 & 0 & 0 \\ 0 & 0 & 1 & 0 \end{bmatrix}, B_2 = \begin{bmatrix} 20.4709 & 0.0224 \\ 0.9287 & 0 \\ -18.5670 & 0 \\ 0 & 0 \end{bmatrix}$  $\alpha = 13.2^{\circ} \qquad A_{3} = \begin{bmatrix} 116.6704 & 18.9110 & 0 & -7.9941 \\ -234.6434 & -38.0412 & 8.5 & -5.6687 \\ -51.7983 & -8.4054 & 0 & 0 \\ 0 & 0 & 1 & 0 \end{bmatrix}, B_{3} = \begin{bmatrix} 12.1215 & 0.0224 \\ -16.5224 & 0 \\ -18.5670 & 0 \\ 0 & 0 \end{bmatrix}$  $\alpha = 14^{\circ} \qquad A_{4} = \begin{bmatrix} 264.7074 & 42.3325 & 0 & -7.9941 \\ -84.6038 & -13.5340 & 8.5 & -5.6687 \\ -54.9460 & -8.7948 & 0 & 0 \\ 0 & 0 & 1 & 0 \end{bmatrix}, B_{4} = \begin{bmatrix} 20.2976 & 0.0224 \\ -2.8159 & 0 \\ -18.567 & 0 \\ 0 & 0 \end{bmatrix}$  $\alpha = 20^{\circ} \qquad A_5 = \begin{bmatrix} 329.1698 & 49.0684 & 0 & -7.9941 \\ -221.6692 & -33.0466 & 8.5 & -5.6687 \\ -78.5534 & -11.7154 & 0 & 0 \end{bmatrix}, B_5 = \begin{bmatrix} 18.7023 & 0.0224 \\ -8.3752 & 0 \\ -18.567 & 0 \\ 0 & 0 \end{bmatrix}$ 

**Table 4.** State-space models vs angle-of-attack α

#### 3.2 Definition of fractional derivation

The fractional-order derivative of order  $\mu \in R$  in the sense of Riemann–Liouville is given as:

$$_{RL}D_{t_0}^{\mu}f(t) = \frac{1}{\Gamma(n-\mu)} \frac{d^n}{dt^n} \int_{t_0}^t (t-\tau)^{n-\mu-1} f(\tau) d\tau$$
 (16)

where  $\Gamma$  (.) is Euler's gamma function and  $n-1 < \mu < n, n \in \mathbb{R}^+$ .

It is well known that industrial controlled processes are habitually discretised, that justifies the approximation of Equation (16). The literature proposes many numerical tools for fractional-order continuous and discrete differential equations [38]. In our work, we are concerning only with integrator and derivative approximation.

### 3.3 Singularity functions

In this work, and in order to implement fractional-order models, we will use the so-called singularity function method developed by Charef et al. [39].

#### 3.3.1 Fractional-order integrator approximation

The transmittance representing the fractional-order integrator is approximated in the frequency domain by an irrational transfer function as:

$$G_I(s) = \frac{1}{s^{\mu}} \tag{17}$$

such that  $0 < \mu < 1$ .

In an operational frequency band  $[\omega_b, \omega_h]$ , it can be modelled by a fractional power pole (FPP) whose transmittance is:

$$G_{I}(s) = \frac{K_{I}}{\left(1 + \frac{s}{\omega_{c}}\right)^{\mu}} \tag{18}$$

Suppose that for  $\omega \in [\omega_b, \omega_h]$ , with  $\omega >> \omega_c$  therefore

$$G_I(s) = \frac{K_I}{\left(\frac{s}{\omega_c}\right)^{\mu}} = \frac{K_I \omega_c^{\mu}}{s^{\mu}} = \frac{1}{s^{\mu}}$$
(19)

were  $K_I = \frac{1}{\omega_c^{\mu}}$  and  $\omega_c$  is the -3mdB frequency corner of the FPP, which is computed based on the low frequency  $\omega_l$ , as  $\omega_c = \sqrt{10^{\frac{\varepsilon}{10\omega}} - 1}$  were  $\varepsilon$  is the highest allowed gap between the slopes of the fractional-order integrator of Equation (17) and the FPP of Equation (18) in the considered frequency operational band  $(\omega_l, \omega_h)$ .

The FPP of Equation (18) and equally the integrator have to be modeled by means of a linear time-invariant system and for that aim we have to approximate its transmittance by a rational one. This method implies the approximation the  $-20\mu$  dB/dec slope on the Bode plot of the FPP by a set of alternative slopes of -20 dB/dec and 0 dB/dec equivalent to alternative poles and zeros on the negative part of the real axis of the complex plane such that  $p_0 < z_0 < p_1 < z_1 < \ldots < z_{N-1} < p_N$ ; Hence, the approximation is given by

$$G_{I}(s) = \frac{K_{I}}{\left(1 + \frac{s}{\omega_{c}}\right)^{\mu}} = K_{I} \frac{\prod_{i=0}^{N-1} \left(1 + \frac{s}{z_{i}}\right)}{\prod_{i=0}^{N} \left(1 + \frac{s}{p_{i}}\right)}$$
(20)

Now by making use of a simple graphical technique that begins with the error specification y in decibels and the frequency band  $\omega_{max}$ , which can be  $100\omega_h$ , the parameters  $a, b, p_0, z_0$  can be computed as [40]

$$a = 10^{\frac{y}{10(1-\mu)}}, b = 10^{\frac{y}{10\mu}}$$

with:

$$p_0 = \omega_c \sqrt{b}, \ z_0 = ap_0$$

The poles  $p_i$  and the zeros  $z_i$  of Equation (20) are in a form of geometric progression. We can then obtain them based on the above parameters as

$$p_i = (ab)^i p_0, \text{ for } i = 0, 1, \dots, N$$
  
 $z_i = (ab)^i a p_0, \text{ for } i = 0, 1, \dots, N - 1$  (21)

with

$$N = \text{Integer} \left[ \frac{\log \left( \frac{\omega_{max}}{p_0} \right)}{\log (ab)} + 1 \right] + 1$$
 (22)

It results that the fractional-order integrator is equivalent to a rational transfer function expressed as

$$G_{I}(s) = \frac{1}{s^{\mu}} = \frac{K_{I}}{\left(1 + \left(\frac{s}{\omega_{c}}\right)\right)^{\mu}}$$
(23)

So  $G_I(s)$  can be approximated as follow

$$G_{I}(s) = K_{I} \frac{\prod_{i=0}^{N-1} \left(1 + \frac{s}{(ab)^{i}ap_{0}}\right)}{\prod_{i=0}^{N} \left(1 + \frac{s}{(ab)^{i}p_{0}}\right)} = \sum_{i=0}^{N} \frac{h_{i}}{\left(1 + \frac{s}{(ab)^{i}p_{0}}\right)}$$
(24)

## 3.3.2 Fractional-order derivative's approximation

The fractional-order derivative equivalent Laplace-domain transmittance is expressed by the following irrational transmittance:

$$G_D(s) = s^{\mu} \tag{25}$$

where  $s = j\omega$  is the complex frequency and  $\mu$  is a positive real number such that  $0 < \mu < 1$ .

In the considered operational frequency band of  $[\omega_b, \omega_h]$ , this fractional-order operator can be represented by a fractional power zero (FPZ) whose transmittance is the following,

$$G(s) = K_D \left( 1 + \frac{s}{\omega_c} \right)^{\mu} \tag{26}$$

Suppose that for  $\omega \in [\omega_b, \omega_h]$ , with  $\omega >> \omega_c$  therefore

$$G_D(s) = K_D \left( 1 + \frac{s}{\omega_c} \right)^{\mu} \tag{27}$$

Were  $K_D = \omega_c^{\mu}$ .

Following the preceding approach, the approximation of the FPP [39], the fractional-order derivative can be approximated by a rational transmittance represented in the operational frequency band by

$$G_D(s) = s^{\mu} = K_D \left( 1 + \frac{s}{\omega_c} \right)^{\mu} \approx K_D \frac{\prod_{i=0}^{N} \left( 1 + \frac{s}{(ab)^i z_0} \right)}{\prod_{i=0}^{N} \left( 1 + \frac{s}{(ab)^i a z_0} \right)}$$
(28)

with

$$a = 10^{\frac{y}{10(1-\mu)}}, b = 10^{\frac{y}{10\mu}}$$

and:

$$z_0 = \omega_c 10^{\left(\frac{y}{20\mu}\right)}, \ p_0 = az_0$$

The zeros  $p_i$  and the poles  $z_i$  of the rational function approximation are given as:

$$z_i = (ab)^i z_0, \ pouri = 0, 1, \dots, N$$
  
 $p_i = (ab)^i a z_0, \ pouri = 0, 1, \dots, N$  (29)

with

$$N = \text{Integer} \left[ \frac{\log \left( \frac{\omega_{max}}{p_0} \right)}{\log (ab)} + 1 \right] + 1 \tag{30}$$

#### 3.4 Fractional-order PID controller (FOPID)

Since the pioneering work of Podlubny [37] in 1999, many researchers and engineers have been attracted to the fractional order PID controller for its augmented flexibility and performance enhancement [41–43]. The FOPID controller used in this work is given by the following transfer function:

$$C_{PID}(s) = K_p \left( 1 + \left( \frac{1}{T_i s} \right)^{\lambda} + (T_d s)^{\mu} \right)$$
(31)

where  $\lambda$ ,  $\mu$  are positive real numbers.

### 4.0 Lqr controller

The well-known LQR is able to stabilise the feedback control closed-loop with optimal gains and offer high-performance synthesis of control systems [44]. In our context, it is used with the aim of control-ling the UAV altitude. MATLAB/Simulink is the simulation platform allowing the design and tuning of the LQR regulator and the simulation to UAV identified model. LQR is based on the theory of optimal control whose objective is to minimise a cost function by optimising a dynamic system, precisely, minimising the deviation of the UAV altitude.

In fact, the main control objective is to achieve certain closed-loop poles that define some desired performance measures (response time, overshoot level, etc.) by placing the closed-loop system eigenvalues in a desired location using a feedback gain. Unfortunately, this statement is not so useful for practical application. The reason is that such a level of performance might require a control signal that is too large for a physical actuator to generate. Such a feedback gain would not be realisable from implementation point of view. In order to find a trade-off between performance and control signal magnitude, LQR control design is a good solution to overcome such problems [45].

One of its main advantages is its easy design and increased state variables accuracy. This property guarantees the stability of the control system [46, 47].

Let us consider an LTI system, expressed as

$$\dot{x} = Ax + Bu + G\delta \tag{32}$$

where x is the state vector, u the control signal and  $\delta$  a disturbance.

Let a state variable feedback regulator be,

$$u = -Kx \tag{33}$$

where *K* is the matrix of the state feedback gain.

In order to optimise it, one has to determine the control input u, which minimises the performance index  $J_{LQR}$ . This later represents the necessary performance characteristic as well as the controller input constraint. The optimal controller has to minimise the following performance index [48],

$$J_{LQR} = \int_0^\infty \left( x'Qx + u'Ru \right) dt \tag{34}$$

where *K* is given by;

$$K = R^{-1}B'P \tag{35}$$

and P is a matrix that satisfies the reduced-matrix Riccati equation,

$$A'P + PA - PBR^{-1}B'P + O = 0 (36)$$

Then the feedback regulator,

$$u = -\left(R^{-1}B'P\right)x\tag{37}$$

Altitude and airspeed outputs are subtracted from the desired reference altitude and airspeed to produce an error signal. Then, the control signals generated by the LQR and FOPID controllers are combined at the input of the UAV system.

These final control signals are further passed through saturation blocks, which represent limitations in aileron deflection angle ( $-12 \ deg < \delta_e < 12 \ deg$ ) and throttle opening ( $0 < \delta_T < 1$ ).

# 5.0 Robust gain-scheduled control system design

Gain scheduling is a particularly appreciated control technique in industrial applications. This is due to the possible application of intuitive approaches and its simple implementation. However, its principal drawback is the lack of theoretical stability tools [49, 50].

Automation engineers often deal with systems whose model is unique and fixed or slowly varying over time. But when tackling more complex systems, models can vary in a variety of other ways: configuration changes, system faults, measurement and actuator noise, external disturbances and parameter variations.

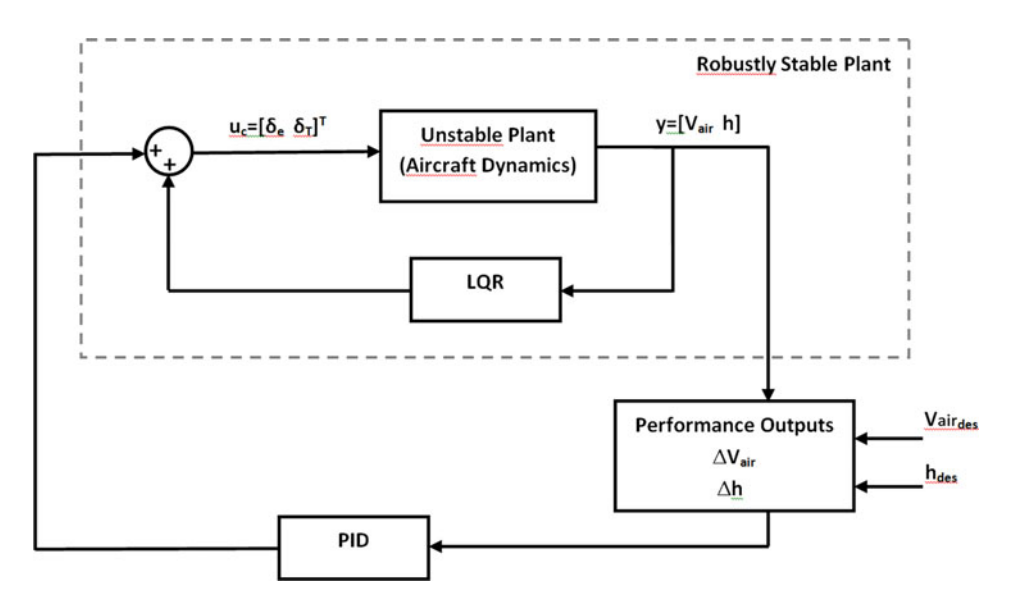


Figure 2. Block diagram of the proposed controller.

In general, complex systems operate in multiple environments that may abruptly change from a context to another as is often the case with aircraft and UAV. The system model depends on a variable parameter, which allows the use of LPV systems theory leading to a set of linear models that become active for certain values of this parameter [51].

If models are available for the different discretised parameters values, the corresponding regulators may be designed apriori. While the system is operating, we have to identify the actual parameter value in order to determine the adapted regulator.

Based on these two ideas, the proposed control strategy is to determine the best model for the current measured or estimated parameter value at every moment and use the corresponding regulator.

For the switching, the problem is to determine when the current parameters values are not satisfactory (that is, when to switch) and with which one we have to replace it (that is, switch to what). For the adjustment, the problem is to determine the law with which the parameter value has to be adjusted at every time.

In this work, linear control solutions are used to supervise the UAV's longitudinal movements with LPV representation for a set of its possible models. LQR method with the PID controller is used to guarantee the stability of the system and a good tracking performance. This technique has been proposed in several studies for processes with invariant models [52, 53].

The main objective of this mixed control is to take benefit from the LQR optimal setting that stabilises the first control loop. Then, the fractional-order PID controller becomes easier to adjust with better performance in tracking the reference input signals. Figure 2 represents the block diagram of the proposed controller for longitudinal controller.

Figure 3 represents the proposed control method. The plant to be controlled has an input u and an output y. The aim of this work is to force the tracking error  $e = y_r - y$  to converge to zero, where  $y_r$  is the reference signal.

## 5.1 Design of the set of combined controllers

We suppose that the LPV model of the system can be represented by a set of  $\nu$  linear models to be identified in advance, indicated by  $M_j$ ,  $j = 1, ...\nu$ . For each model  $M_j$  one has to design a combined controller  $C_j$  as represented in Fig. 2. This synthesis is realised in two steps:

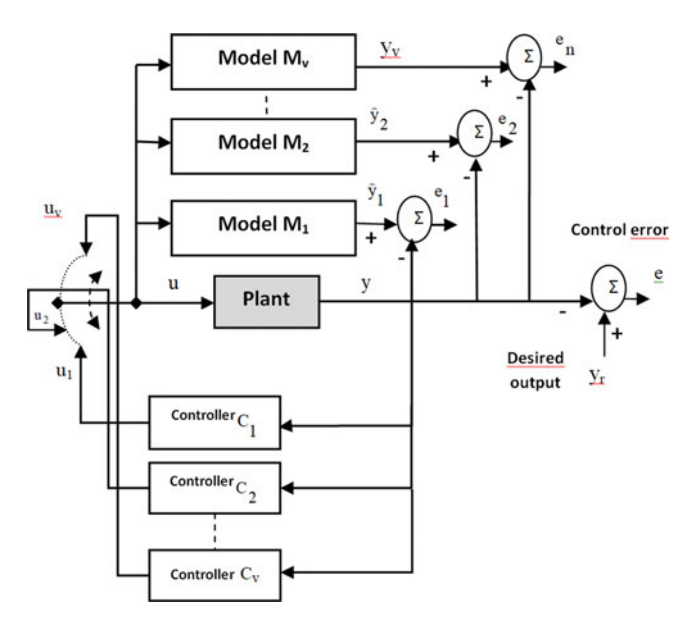


Figure 3. Gain-scheduled control algorithm.

- 1. First, we have to design an LQR controller as detailed in Equations (32) to (36). The closed-loop model obtained by LQR control is  $(M_{LQR})_j$ . This step system should be stabilised by the first controller for which the parameters are optimised using a meta-heuristic technique, here the PSO technique.
- 2. In a second step, we will design a fractional-order PID controller for each LQR closed-loop system in order to enhance the performance of the overall controlled system and guarantee its stability and robustness. For each model  $(M_{LQR})_j$  a controller  $(C_{FOPID})_j$  is designed as in Equation (30) and its parameters are optimised using the PSO technique

## 5.2 Moving time switching law

In control and measurement, a switching law typically dictates which number of control, from a given list of controllers, is chosen to be used at a particular time instant, depending on particular given conditions.

In the present work, the decision when and to which controller should be the switching is based on a cost function minimisation  $min_j(J_j(t))$  for each regulator  $C_j$  at every instant. It implies the evaluation of each model for each sample time. We propose the following cost function represented by a moving time window of length T formulated as:

$$J_{j}(t) = \int_{t}^{t-T} e_{j}^{2}(t)$$
 (38)

At every instant, the performance factors  $\{J_j(t)\}$  are compared allowing the switching decision, as explained in the algorithm of Fig. 3.

Following the switch, the system is blocked for a  $T_{min} > 0$  length waiting period, and after that, the regulator that indicates the minimum cost function is pointed out (switching target) to be applied to the plant. This waiting period is motivated by preventing the system from too fast arbitrary switching [7, 54].

## 5.3 Stability analysis

The following stability theorem states the ability of the proposed adaptive robust gain-scheduled controller to stabilise the UAV system.

**Table 5.** Different models of the LPV models of altitude and velocity of the UAV

UAV Altitude	UAV Velocity
$H(s) = \frac{20,49s^3 + 416,1s^2 - 2542s + 1,795e04}{s^4 + 48,54s^3 + 581,2s^2 + 3075s + 8812}$	$V(s) = \frac{0,01826s^3 + 0,3636s^2 + 50,56s + 154,7}{s^4 + 48,54s^3 + 581,2s^2 + 3075s + 8812}$
$H_1(s) = \frac{16,92s^3 + 451,2s^2 - 598s + 1,853e04}{s^4 + 123,7s^3 + 1278s^2 + 4964s + 9094}$	$V_1(s) = \frac{0,01826s^3 + 0,02458s^2 + 26,54s + 55,8}{s^4 + 123,7s^3 + 1278s^2 + 4964s + 9094}$
$H_2(s) = \frac{11,08s^3 + 475,5s^2 + 1055s + 1,495e04}{s^4 + 160,2 + 1278^2 + 5412s + 7341}$	$V_2(s) = \frac{0,01826s^3 - 0,5634s^2 + 23,18s + 5,182}{s^4 + 160,2 + 1278s^2 + 5412s + 7341}$
$H_3(s) = \frac{20,49s^3 + 804s^2 - 3499s + 3,351e4}{s^4 + 90,79s^3 + 1058s^2 + 5593s + 1,971e4}$	$V_3(s) = \frac{0,01826s^3 + 0,6041s^2 + 66,64s + 294}{s^4 + 90,79s^3 + 1058s^2 + 5593s + 1,971e4}$
$H_4(s) = \frac{14,04s^3 + 851,8s^2 + 1422s + 3,004e04}{s^4 + 259,7s^3 + 2222s^2 + 9835s + 1,496e04}$	$V_4(s) = \frac{0,01826s^3 - 0,3107s^2 + 45,87s + 56,22}{s^4 + 259,7s^3 + 2222s^2 + 9835s + 1,496e04}$
$H_5(s) = \frac{17,65s^3 + 1222s^2 - 64,81s + 4,887e4}{s^4 + 305,3s^3 + 2813s^2 + 1,317e04s + 2,448e4}$	$V_5(s) = \frac{0,01826s^3 + 0,5572s^2 + 74,15s + 188,2}{s^4 + 305,3s^3 + 2813s^2 + 1,317e04s + 2,448e4}$

**Theorem 1.** The UAV with LPV model described by Equation (13) controlled using the gain-scheduled adaptive controller based on LQR - FOPID controllers Equation (30) and Equation (36), with the switching law presented in Fig. 3, is exponentially stable.

**Proof.** The proof is similar to the one in Ref. (7).

# 6.0 Application for uav airspeed and altitude control

In this section we will apply the proposed gain scheduled strategy to the control of the UAV Altitude and velocity. Five different models are considered for modelling the LPV system. Both integer order and fractional order controllers are considered for either the altitude or velocity of the plane, and the results are given in the ideal case and in presence of random disturbances.

Consider a real LPV system given by its state space linearised model presented in Section 2.1 and given in the form of Equation (31).

We suppose that the plant parameters will change periodically between five constant values of the angle-of-attack  $\alpha$ , such that:  $\alpha = [6, 9^{\circ} (plant) \ 7, 5^{\circ} \ 7, 9^{\circ} \ 13, 2^{\circ} \ 14^{\circ} \ 20^{\circ}].$ 

Then we have five linear models representing the LPV plant whose different linear transmittances are given in Table 5.

First of all, we apply LQR feedback controller for the five system's models in (using state space formula), we get stability of the system, like mentioned in Table 6.

Then, for each LQR closed-loop transfer function, we compute a fractional-order PID controller as in Equation (30).

Table 7 gives the regulators of the UAV altitude. Wheras, Table 8 gives the regulators of the UAV velocity.

#### 6.1 Control with ideal conditions (without noises)

We begin the UAV control experiment by considering that the plant is in ideal conditions. This means that we minimise external factors like wind, obstacles, additive actuators' and sensors' noises and signal interference, which enables more precise navigation and manoeuvers.

#### 6.1.1. Simulations of UAV altitude

In nominal flight conditions, the designed controllers must achieve stabilisation of the UAV altitude around  $h \approx 150m$ . This is the normal flying altitude.

	o. 1 of the controllers	serjor or	i ammac	
$\alpha(t)$	LQR gain			
$\alpha = 6,9^{\circ} (plant)$	$k = \begin{bmatrix} 13,2607 \\ 4,6696 \end{bmatrix}$	2, 1650 1, 1887	2, 0336 1, 1080	9, 6766 -3, 3272
$\alpha = 7,5^{\circ}$	$k_1 = \begin{bmatrix} 13,9835 \\ 1,0148 \end{bmatrix}$	2, 2215 0, 2420	0, 7903 0, 1145	$\begin{bmatrix} 6,1841 \\ -0,2807 \end{bmatrix}$
$\alpha = 7,9^{\circ}$	$k_2 = \begin{bmatrix} 15,7482\\0,9253 \end{bmatrix}$	2, 5059 0, 1506	0, 6756 0, 0783	5, 3712 0, 4114
$\alpha = 13, 2^{\circ}$	$k_3 = \begin{bmatrix} 19,5086 \\ 3,7759 \end{bmatrix}$	2, 7137 0, 8524	1, 2013 0, 5304	$\begin{bmatrix} 8,9341 \\ -2,9030 \end{bmatrix}$
$\alpha=14^{\circ}$	$k_4 = \begin{bmatrix} 26,3068\\1,5645 \end{bmatrix}$	3, 7558 0, 2627	0, 6735 0, 0844	5, 7547 0, 0815
$\alpha = 20^{\circ}$	$k_5 = \begin{bmatrix} 34,9991 \\ 2,3904 \end{bmatrix}$	4, 7663 0, 4183	0,7157 1,1090	$\begin{bmatrix} 6,2817 \\ -0,4224 \end{bmatrix}$

Table 6. FOPID controllers set for UAV altitude

Table 7. FOPID controllers set for UAV altitude

Integer order model	fractional order model	
$C_1(s) = 0.0092 + \frac{0.3249}{s} + 0,00075s$	$\lambda = 0, 8; \mu = 0.6$	
$C_2(s) = 0.1379 + \frac{0.1139}{s} + 0,02802s$	$\lambda = 0, 8; \mu = 0.6$	
$C_3(s) = 0.0701 + \frac{0.1006}{s} + 0,01768s$	$\lambda = 0, 8; \mu = 0.6$	
$C_4(s) = 0.1624 + \frac{0.2099}{s} + 0,04071s$	$\lambda = 0, 8; \mu = 0.6$	
$C_5(s) = 0.06563 + \frac{0.000553}{s} + 0,1741s$	$\lambda = 0, 8; \mu = 0.6$	

Table 8. FOPID controllers set for UAV velocity

Integer-Order Model	Fractional-Order Model	
$C_1(s) = 2.085 + \frac{8.761}{s} + 0{,}222s$	$\lambda = 0, 8;  \mu = 0.6$	
$C_2(s) = 13,79 + \frac{11,39}{s} + 2,802s$	$\lambda = 0, 8;  \mu = 0.6$	
$C_3(s) = 0.3485 + \frac{4,3485}{s} + 0,000875s$	$\lambda = 0, 8; \mu = 0.6$	
$C_4(s) = 1.5560 + \frac{4,166}{s} + 0,001062s$	$\lambda = 0, 8;  \mu = 0.6$	
$C_5(s) = 1.8690 + \frac{6,0520}{s} + 0,023s$	$\lambda = 0, 8;  \mu = 0.6$	

In our experimental test we will apply gradual reference steps for the desired altitude  $h_{des}$  to test the reference tracking and closed-loop system performance.

The simulation results of the UAV altitude h control in ideal conditions (without additive noises) using the proposed robust gain-scheduling controller are given in Fig. 4.

It can be observed from Fig. 4(a) that the altitude response tracks the reference signal with rapidity and precision. The fractional order case does not present any overshoot, while in the integer case, there are important peaks at the steps instants. The same remark is observable on the control signal in Fig. 4(b) which is smoother with the fractional order controller which implies a reduction of the energy costs.

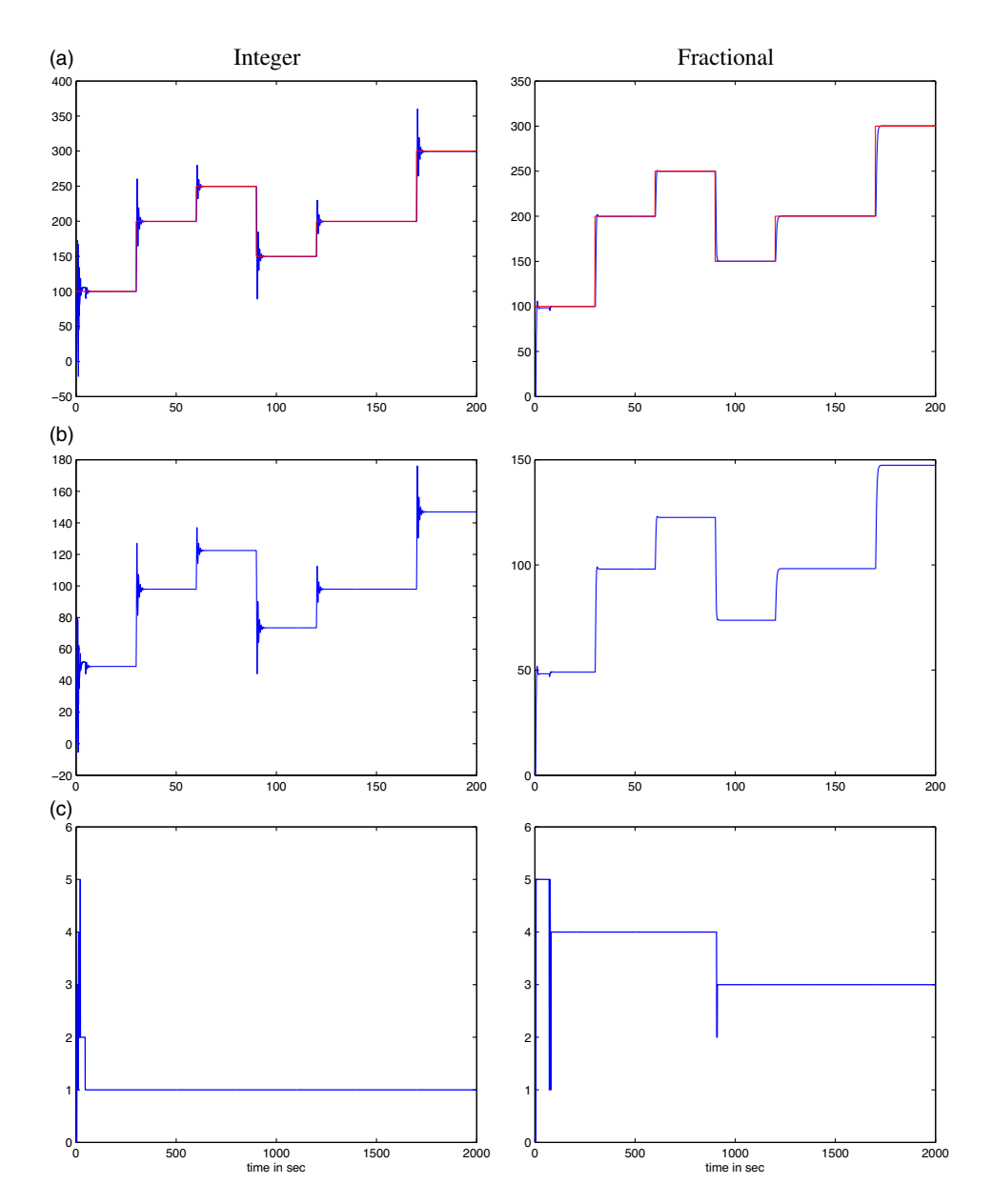


*Figure 4.* UAV altitude response in ideal conditions with integer and fractional PID IDLQR controller: (a) Output signal h (b) Control signal (c) Switching index.

Besides, one can see that the switching system is more active in the fractional case in Fig. 4(c), which improves the precision of the control comparatively to the integer case where the controller stabilises with the model 1 after a short time.

#### 6.1.2. Simulations of UAV velocity

In nominal flight conditions, the designed controllers must achieve stabilisation of airspeed (velocity) around  $V_{air} \approx 10m/s$ . This is the normal cruise speed.

In our experimental test we will apply gradual reference steps for  $V_{air_{des}}$  to test the reference tracking and closed-loop system performance.

The simulation results of the UAV velocity (airspeed  $V_{air}$ ) control in ideal conditions (without additive noises) using the proposed robust gain-scheduling controller are given in Fig. 5.

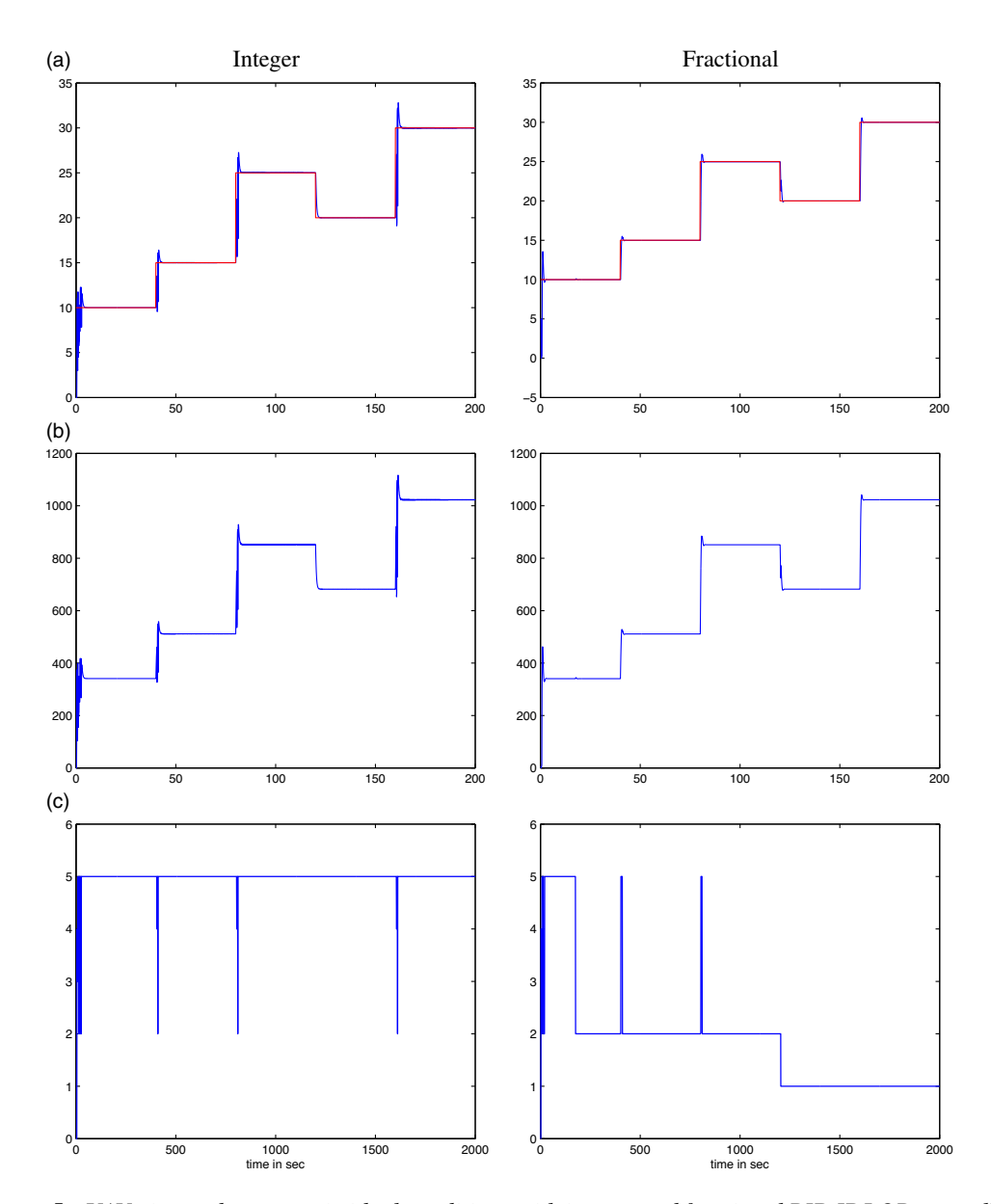


**Figure 5.** UAV airspeed response in ideal conditions with integer and fractional PID IDLQR controller: (a) Output signal  $V_{air}$  (b) Control signal (c) Switching index.

It can be noticed again from Fig. 5(a) that the velocity response tracks the reference signal with good temporal performance. The overshoot in the fractional-order response is very small and negligible comparatively to the integer case. The same comment can be stated for the control signal in Fig. 5(b) which is smoother with the fractional order controller which also implies a reduction of the energy costs. Besides, the switching system is more dynamic in the fractional-order case in Fig. 5(c), which allows better adaptation and tracking performance.

# 6.2 Case of UAV with sensors random noises

In this second experiment setting, the system is supposed to be subject to additive output random measure noises.

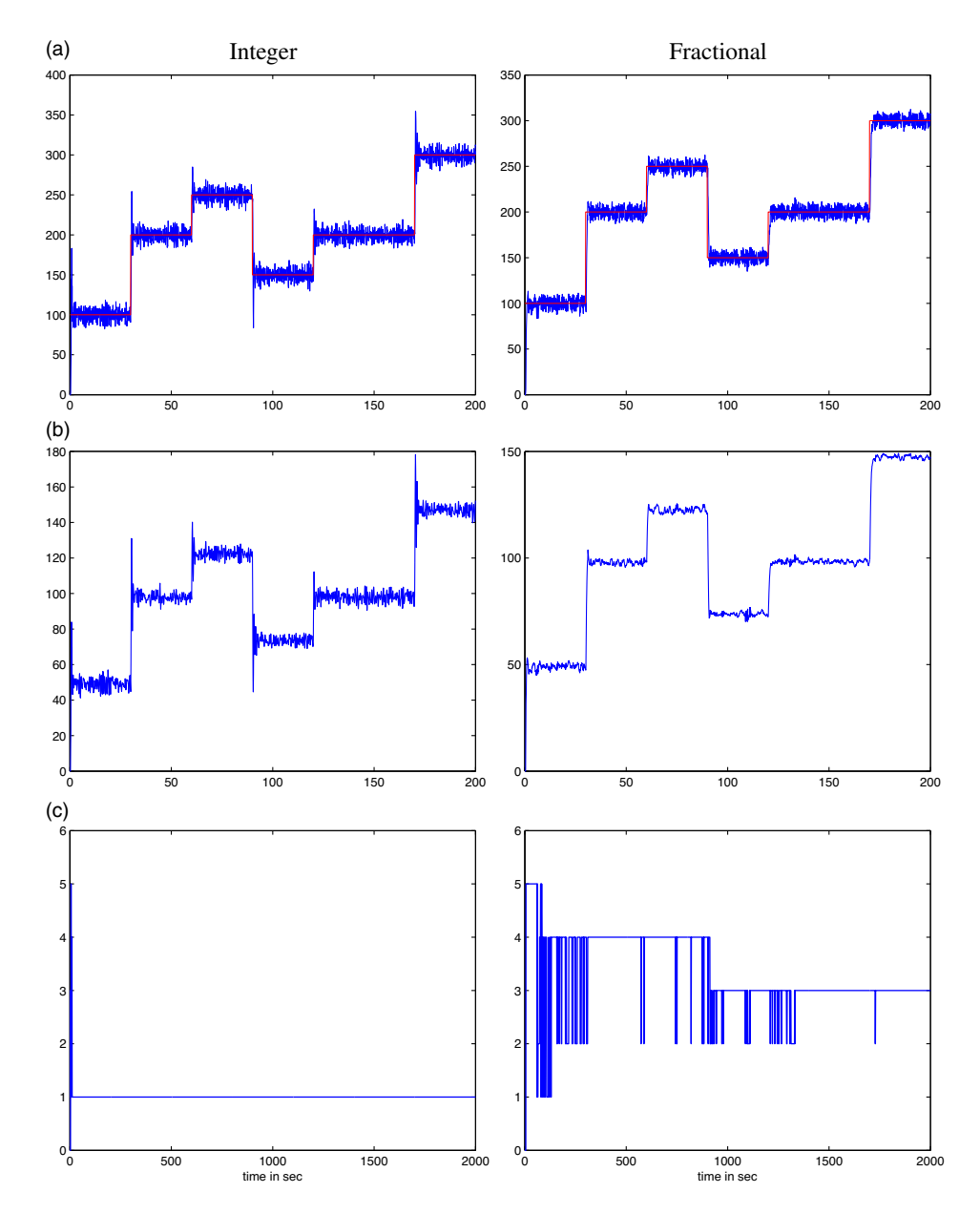


**Figure 6.** UAV altitude response presence of sensors random noises with integer and fractional PID IDLQR controller: (a) Output signal h (b) Control signal (c) Switching index.

#### 6.2.1 Simulations of UAV altitude (noisy case)

The simulation results of the UAV altitude control that is affected by random noises using the proposed robust gain-scheduling controller are given in Fig. 6.

The altitude output signal in Fig. 6(a) shows a lower level of oscillations in the fractional-order response with the absence of picks that are remarkable in the integer-order case. This fact is still more visible for the control signals in Fig. 6(b). Same for the switching system, which is more active in the fractional-order case as can be seen in Fig. 6(c),

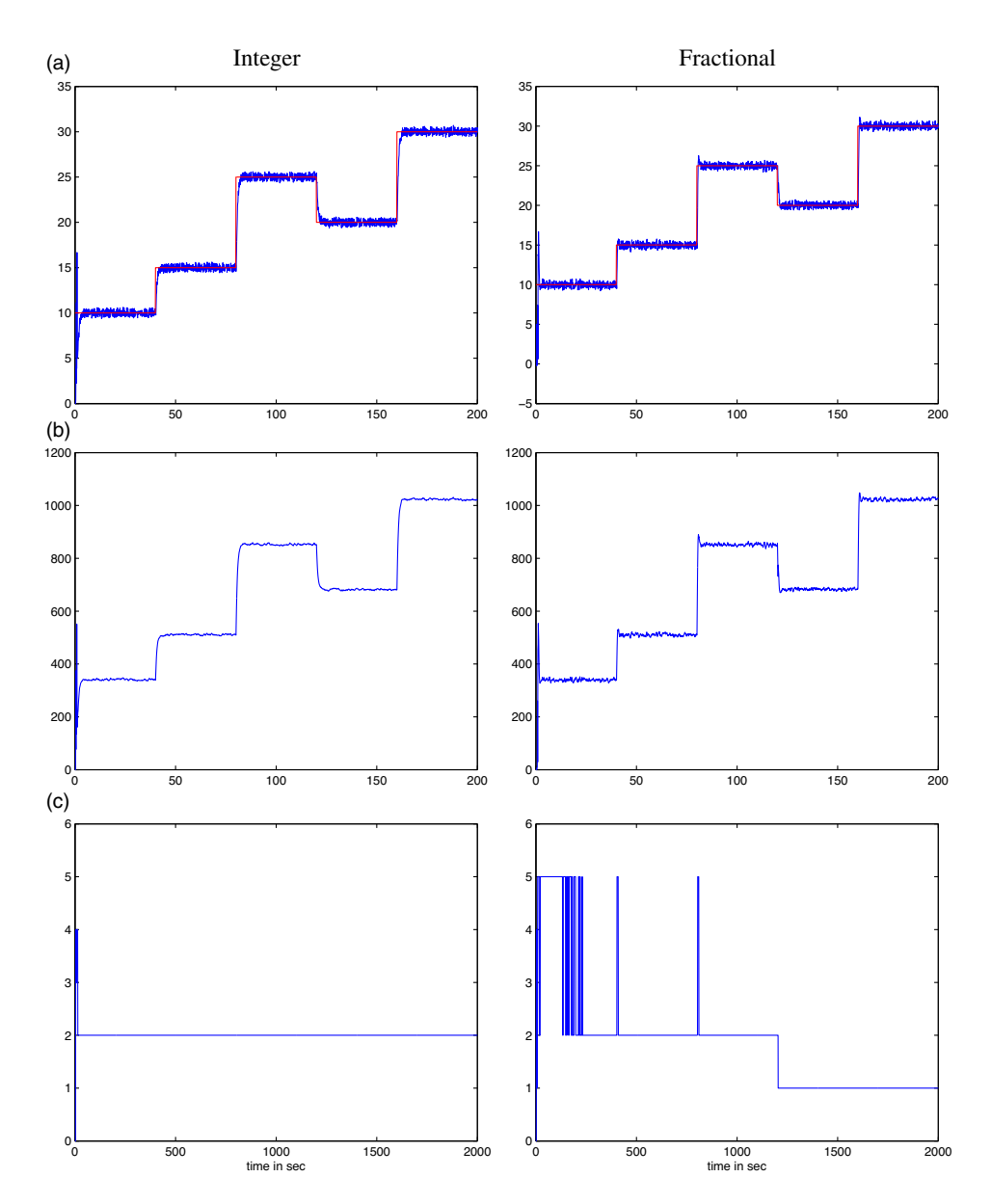


**Figure 7.** UAV airspeed response in ideal conditions with integer and fractional PID IDLQR controller: (a) Output signal  $V_{air}$  (b) Control signal (c) Switching index.

# 6.2.2 Simulations of UAV velocity (noisy case)

The simulation results of the UAV airspeed control affected with sensor's random noises using the proposed robust gain-scheduling controller are given in Fig. 7.

The airspeed output signal in Fig. 7(a) shows a similar level of oscillations in the fractional-order response with the absence of high picks. The same remark can be given for the control signals in Fig. 7(b). However, it is obvious that there only a few switches in the beginning of simulation for the integer order controller, whereas many controllers and models are involved with the fractional order response as could be seen in Fig. 7(c),

#### 7.0 Conclusion

In this paper, a new innovative adaptive control design based on gain-scheduled fractional-order PID + LQR controllers for a class of LPV systems is presented. An adaptive switching law with a fixed time-window based on the plant output performance index is used to manage the change between the pre-designed controllers. The proposed robust adaptive control strategy is very convenient for the control of UAV systems airspeed and altitude, as they are perfectly described by LPV models.

LQR control method is used to stabilise the linear models of the plant then fractional-order PID controllers are designed for each closed-loop LQR system based on the PSO optimisation method.

The analysis of stability is performed and demonstrates that the controlled system tracks the reference signal perfectly. This combined scheduled control has been applied with success to a real case study involving the control of both the altitude and the airspeed of a UAV system with satisfactory results in terms of time performance and robustness against measurement noises.

The strategy, which consists of a switching law between five predesigned combined LQR-FOPID controllers depending on a variable parameter measure of the LPV plant model, proved its effectiveness in tracking desired altitude and airspeed.

Furthermore, this fractional-order control method demonstrated a satisfactory performance in terms of settling time, overshoots reduction and robustness against additive noises. The switching law is more active in the case of fractional-order controller, which allows a better adaptability and ability to reduce the tracking error.

Future research will focus on combining fractional-order modeling and fractional adaptive control in order to enhance the closed-loop control performance and robustness versus disturbances and model uncertainties.

Competing interests. The author(s) declare none.

## References

- [1] Giarre, L., Bauso, D., Falugi, P. and Bamieh, B. LPV model identification for gain scheduling control: an application to rotating stall and surge control problem, *Control Eng. Pract.*, 2006, **14**, (4), pp 351–361.
- [2] Kvieska, P.N., Lebret, G. and Ait-Ahmed, M. Gain scheduled LPV systems global vision and stability results, In Workshop on Advanced Control and Diagnosis, Nov. IAR/ACD08, Coventry, United Kingdom, 2008, pp 1–7.
- [3] Zhang, S., Yang, J.J. and Zhu, G.G. LPV gain-scheduling control of an electronic hrottle with experimental validation, In 2014 American Control Conference, ACC, IEEE, 4-6, Portland, OR, USA, 2014, pp 190–195.
- [4] Å ström, K.J. and Wittenmark, B. Adaptive Control, Addison-Wesley, 1994, Boston, USA.
- [5] Huang, B., Lu, B. and Li, Q. A proportional-integral-based robust state-feedback control method for linear parameter-varying systems and its application to aircraft, *J. Aerosp. Eng.*, 2019, 233, (12), pp 4663–4675.
- [6] Rahme, S., Abbas, H.A., Meskin, N., Tóth, R. and Mohammadpour, J. Reduced LPV model development and control of a solution copolymerization reactor, In *IEEE Conference on Control Applications Part of 2015 IEEE Multi-Conference on Systems and Control*, IEEE, 21-23, Sydney, Australia, 2015, pp 1044–1050.
- [7] Kissoum, S., Ladaci, S. and Charef, A. Smith predictor PID-based robust adaptive gain-scheduled control for a class of fractional order LPV systems with time delays, *Int. J. Dyn. Control*, 2023, 11, pp 3096–3108.
- [8] Kumar, E.V. and Jerome, J. Robust LQR controller design for stabilizing and trajectory tracking of inverted pendulum, Procedia Eng., 2013, 64, pp 169–178.
- [9] Ahmad, F., Kumar, P., Bhandari, A., and Patil, P.P. Simulation of the quadcopter dynamics with LQR based control, *Mater. Today:*. *Proc.*, 2020, **24**, (2), pp 326–332.
- [10] Setyawan, G.E., Kurniawan, W. and Gaol, A.C.L. Linear quadratic regulator controller (LQR) for AR. drone's safe landing, In *International Conference on Sustainable Information Engineering and Technology (SIET)*, 28-30, IEEE, Lombok, Indonesia, 2019, pp 228–233.
- [11] Elkhatem, A.S. and Engin, S.N. Robust LQR and LQR-PI control strategies based on adaptive weighting matrix selection for a UAV position and attitude tracking control, *Alex. Eng. J.*, 2022, **61**, (8), pp 6275–6292.
- [12] Balaska, H., Ladaci, S., Schulte, H., and Djouambi, A. Adaptive cruise control system for an electric vehicle using a fractional order model reference adaptive strategy, *IFAC-PapersOnLine*, 2019, 52, (13), pp 194–199.
- [13] Ladaci, S. and Charef, A. On fractional adaptive control, Nonlinear Dyn., 2006, 43, (4), pp 365–378.
- [14] Seghiri, T., Ladaci, S. and Haddad, S. Fractional order adaptive MRAC controller design for high-accuracy position control of an industrial robot arm, *Int. J. Adv Mech Syst.*, 2023, **10**, (1), pp 8–20.
- [15] Bourouba, B., and Ladaci, S. Robust fuzzy adaptive sliding mode stabilization for fractional-order chaos, *Algorithms*, 2018, **14**, (7), p 101.

- [16] Aguila-Camacho, N., Bustos, J.G., López, E.C., Gallego, J.A. and TraviesoTorres, J. Switched fractional order model reference adaptive control for first order plants: a simulation-based study, J Dyn Syst Meas Control, 2022, 144, (4), p 044502.
- [17] Ladaci, S., Khelas, S., Ynineb, A.R., Copot, D. and Ionescu, C.-M. Fractional order MRAC control design for a lightning system based on a fractional order second degree model, *IFAC-PapersOnLine*, 2024, **58**, (12), pp 95–100.
- [18] Di Paola, M., Pinnola, F.P. and Zingales, M. Fractional differential equations and related exact mechanical models, *Comput. Math. Appl.*, 2013, **66**, (5), pp 608–620.
- [19] Lino, P., Maione, G. and Saponaro, F. Fractional-order modeling of high-pressure fluid-dynamic flows: An automotive application, *IFAC-PapersOnLine*, 2015, **48**, (1), pp 382–387.
- [20] Ladaci, S., Loiseau, J.J. and Charef, A. Fractional order adaptive high-gain controllers for a class of linear systems, *Nonlinear Sci. Numer. Simul.*, 2008, **13**, (4), pp 707–714.
- [21] Firouzjahi, M., Naderi, B. and Tabriz, Y.E. The consensus of different fractional-order chaotic multi-agent systems using adaptive protocols, J. Math., 2022, 5129072, pp 1–10.
- [22] Oktay, T. and Coban, S. Simultaneous longitudinal and lateral flight control systems design for both passive and active morphing TUAVs, Elektronika Ir Elektrotechnika, 2017, 23, (5), pp 15–20.
- [23] Oktay, T., Arik, S., Turkmen, I., Uzun, M., and Celik, H. Neural network based redesign of morphing UAV for simultaneous improvement of roll stability and maximum lift/drag ratio, Aircr. Eng Aerosp. Technol.: An International Journal, 2018, 90, (8), pp 1203–1212.
- [24] Arik, S., Turkmen, I. and Oktay, T. Redesign of morphing UAV for simultaneous improvement of directional stability and maximum lift/drag ratio, Adv. Electr. Comput. Eng., 2018, 18, (4), pp 57–62.
- [25] Kose, O. and Oktay, T. Simultaneous design of morphing hexarotor and autopilot system by using deep neural network and SPSA, Aircr. Eng Aerosp. Technol.: An International Journal, 2023, 95, (6), pp 939–949.
- [26] Uzun, M. and Oktay, T. Simultaneous UAV having actively sweep angle morphing wing and flight control system design, Aircr. Eng Aerosp. Technol.: An International Journal, 2023, 95, (7), pp 1062–1068.
- [27] Yesilbas, E., özgür, B., Ozen, E. and Oktay, T. Simultaneous and stochastic design of piston-prop TUAV vertical tail and its autonomous system, *Aircraft Engineering and Aerospace Technology: An Int. J.*, 2025, **97**, (4), pp 395–404.
- [28] Li, Y., Lv, R. and Wang, J. A Control Strategy for Autonomous Approaching and Coordinated Landing of UAV and USV, Drones, 2025, 9, p 480.
- [29] Tsourveloudis, C. and Doitsidis, L. UAV Path Planning and Control: Towards a Complete Mission Management System, In 2025 International Conference on Unmanned Aircraft Systems (ICUAS), Charlotte, NC, USA, 2025, pp. 689–696.
- [30] Zhiping, L. and Fang, T. Model derivation and control system simulation for unmanned aerial vehicle, In Chinese Control and Decision Conference (CCDC), Guiyang, China, 2013, vol. 25, pp 4053–405.
- [31] Ren, W. and Beard, R.W. Trajectory tracking for unmanned air vehicles with velocity and heading rate constraints, *IEEE Trans Control Syst. Technol.*, 2004, **12**, (5), pp 706–716.
- [32] Nelson, R.C. Flight Stability and Automatic Control, WCB/McGraw-Hill, 1998, Singapore.
- [33] Beard, R.W. and McLain, T.W. Small Unmanned Aircraft: Theory and Practice, Princeton University Press, 2012, Princeton, NJ, USA.
- [34] Ergöçmen, B. Reconfigurable Dynamic Control Allocation with SDRE As a FTFC for NASA GTM Design, In 2021 American Control Conference (ACC), New Orleans, LA, USA, 2021, pp. 1378–1383.
- [35] Fahlstrom, P.G. and Gleason, T.J. Introduction to UAV systems, John Wiley & Sons, Ltd, 2012, Oxford, England.
- [36] Botez, R.M. Unmanned aerial system (UAS) modeling, simulation and control, Des., 2022, 6, (5), 78.
- [37] Podlubny, I. Fractional order systems and PI  $^{\lambda}$ D  $^{\mu}$  controllers, *IEEE Trans Autom. Control*, 1999, **44**, (1), pp 208–214.
- [38] Hajiyev, C., Soken, H.E. and Vural, S.Y. Linear quadratic regulator controller design, In State Estimation and Control for Low-cost Unmanned Aerial Vehicles, Springer Cham, 2015, pp 171–200.
- [39] Charef, A., Sun, H.H., Tsao, Y.Y. and Onaral, B. Fractal system as represented by singularity function, *IEEE Trans. Autom. Control*, 1992, 37, (9), pp 1465–1470.
- [40] Ladaci, S. and Bensafia, Y. Indirect fractional order pole assignment based adaptive control, *Eng Sci. Technol. an Int. J.*, 2016, **19**, (1), pp 518–530.
- [41] Edet, E. and Katebi, R. On fractional-order PID controllers, IFAC-PapersOnLine, 2018, 51, (4), pp 739–744.
- [42] Mehra, V., Srivastava, S. and Varshney, P. Fractional-order PID controller design for speed control of dc motor, In 2010 International Conference on Emerging Trends in Engineering and Technology, IEEE, 19-21, Goa, India, 2010, 3, pp 422–425.
- [43] Krishna, P.S. and Rao, P.V.G.K. Fractional-order PID controller for blood pressure regulation using genetic algorithm, *Biomed. Signal Process. Control*, 2024, **88**, (B), p 105564.
- [44] Chacko, S.J., Neeraj, P.C. and Abraham, R.J. Optimizing lqr controllers: A comparative study, *Results Control Optim.*, 2024, 14, p 100387.
- [45] Willis, J., Johnson, J., and Beard, R.W. State-Dependent LQR Control for a Tilt-Rotor UAV, In 2020 American Control Conference (ACC), Denver, CO, USA, 2020, pp. 4175–4181.
- [46] Wang, L., Ni, H., Zhou, W., Pardalos, P.M., Fang, J. and Fei, M. MBPOA-based LQR controller and its application to the double-parallel inverted pendulum system, *Eng. Appl. Artif. Intell.*, 2014, 36, pp 262–268.
- [47] Zhao, D., Yang, X., Li, Y., Xu, L., She, J. and Yan, S. A Kalman–koopman LQR control approach to robotic systems, *IEEE Trans. Ind. Electron.*, 2024, **71**, (12), pp 1–10
- [48] Rui, W., Wang, Y., Song, H., Luo, Z., Huang, Y., textsc Yu, Q., Liu, Z., Wu, K. and Xiao, B. using LQR controller for vertical position control on EAST, *Nucl. Fusion*, 2024, **64**, (066040), pp 1–10.

- [49] Kissoum, S. and Ladaci, S. Robust fractional-order adaptive gain-scheduled control for UAVs altitude with LPV models, In *International Conference on Advanced Engineering in Process Intelligence*, ICAEPI, 28-30 2023, vol. 4, Skikda, Algeria, pp 1–6.
- [50] Hencey, B. and Alleyne, A. Robust gain-scheduled control, In 2010 American Control Conference, ACC, 30 June 2010-02 July 2010, IEEE, Baltimore, MD, USA, pp 3075–3081.
- [51] Leulmi, M.I., Ladaci, S. and Schulte, H. A novel state–space model reference adaptive speed control design for fractional-order model-based wind turbine, *Int. J. Electr. Power Energy Syst.*, 2025, 170, 110599.
- [52] He, J.-B., Wang, Q.-G. and Lee, T.-H. PI/PID controller tuning via LQR approach, Chem. Eng. Sci., 2000, 55, (13), pp 2429–2439.
- [53] Kim, K., Kim, H.-G., Song, Y. and Paek, I. Design and simulation of an LQR-PI control algorithm for medium wind turbine, *Energies*, 2019, **12**, 2248.
- [54] Ladaci, S. and Khettab, K. Fractional order multiple model adaptive control, J. Autom. Syst. Eng, 2012, 6, (2), pp 110–122.